Inorg. Chem. **2003**, *42*, 7593–7601

Inorganic Chemistry
Article

Experimental and Theoretical Electron Density Distribution and Magnetic Properties of the Butterfly-like Complex $[Fe_4O_2(O_2CCMe_3)_8(NC_5H_4Me)_2]\cdot 2CH_3CN$

Jacob Overgaard,[†,‡] David E. Hibbs,[‡] Eva Rentschler,[§] Grigore A. Timco,[||] and Finn K. Larsen*,[†]

Department of Chemistry, University of Aarhus, Langelandsgade 140, DK-8000 Aarhus C, Denmark,
MPI für Strahlenchemie, D-45470 Muelheim, Germany, Institute of Chemistry,
Academy of Sciences of the Republic of Moldova, MD-2028 Chisinau, Moldova, and
School of Chemistry, Building F11, University of Sydney, NSW 2006, Sydney, Australia

Received January 20, 2003

The structure and electron density distribution (EDD) of the carboxylate-bridge iron complex $[Fe^{III}_4(\mu_3\text{-}O)_2(O_2CCMe_3)_8(NC_5H_4Me)_2]\cdot 2CH_3CN$, **1**, has been determined from synchrotron X-ray diffraction data ($R_{int} = 0.025$) collected with the crystal cooled to 16(5) K. At this temperature complex **1** crystallized in the triclinic space group $P\bar{1}$ with cell parameters $a = 12.6926(7)$ Å, $b = 12.9134(8)$ Å, $c = 13.4732(8)$ Å, $\alpha = 115.372(2)°$, $\beta = 107.702(3)°$, and $\gamma = 102.731(2)°$. The theoretical EDD determined from a density functional theory (DFT) single point calculation of an entire molecule of **1** at the experimental geometry has been analyzed and compared to the experimental EDD. The latter is expressed in the framework of a multipolar model with parameters determined by least-squares refinement ($R_w(F^2) = 0.024$) based on the X-ray diffraction data. The central μ_3-oxygen atom in **1** is significantly out of the plane spanned by the three Fe atoms coordinated to this oxygen. Comparison of measures for the bonding geometry around the iron atoms in **1** with the corresponding values for the iron atoms in relevant trinuclear complexes suggests that there are significant differences in the Fe–(μ_3-O) bonds in the two cases. Analyses of both the experimental and theoretical EDDs reveal very significant differences between the two Fe–(μ_3-O) bonds in **1**, with one bond being much more directed and stronger than the other bond. A topological analysis of the EDDs using the atoms in molecules approach also reveals very distinct differences between the properties of the two Fe^{III} atoms. A clear exponential relationship is found between the Laplacian of the experimental density at the bond critical points in the Fe–ligand bonds and their bond lengths. Mössbauer spectroscopy of **1** shows two easily separable doublets corresponding to the two different iron sites. Magnetic susceptibility measurements between 4.2 and 300 K indicate antiferromagnetically coupled Fe^{III} atoms constituting an $S = 0$ ground state.

Introduction

The quest for increasingly detailed knowledge of the mechanisms of non-heme iron-containing enzymes has followed different paths. Spectroscopic methods, in combination with theoretical calculations, have presented many interesting results,[1] as has X-ray diffraction.[2] In particular, the iron−oxo clusters are interesting for their magnetic properties.[3] A large number of polynuclear iron-containing model systems have been prepared, the most proliferate being the μ_3-oxo trinuclear iron carboxylate complexes of general type $[Fe_3O(O_2CR)_6L_3]^zS$, with a wide variety of bridging carboxylates (O_2CR), ligands (L), and possibly solvent molecules (S), where $z = +1$ for Fe^{III}_3 and $z = 0$ for Fe^{III}_2-Fe^{II} metal composition of the compound. Trinuclear iron complexes can undergo oligomerization processes forming e.g. tetranuclear complexes of the so-called butterfly type first reported for iron(III) carboxylates by Ponomarev et al.[4]

---

* To whom correspondence should be sent. E-mail: kre@chem.au.dk.
[†] University of Aarhus.
[‡] University of Sydney.
[§] MPI für Strahlenchemie.
[||] Academy of Sciences of the Republic of Moldova.

(1) Solomon, E. I. *Inorg. Chem.* **2001**, *40*, 3656−3669.

(2) Lippard, S. J. *Angew. Chem., Int. Ed. Engl.* **1988**, *27*, 344−361. (b) Hendrickson, D. N. In *Mixed Valency Systems: Applications in Chemistry, Physics and Biology*; Prassides, K., Ed.; Kluwer Academic Publishers: Dordrecht, 1991; pp 67−90.

(3) (a) Gatteschi, D.; Caneschi, A.; Sessoli, R.; Cornia, A. *Chem. Soc. Rev.* **1996**, *25*, 101. (b) Gatteschi, D.; Sessoli, R.; Cornia, A. *Chem. Commun.* **2000**, 725−732.

(4) Ponomarev, V. I.; Atovmyan, L. O.; Bobkova, S. A.; Turte, K. I. *Dokl. Akad. Nauk. SSSR* **1984**, *274*, 368−372.

10.1021/ic034062c CCC: $25.00

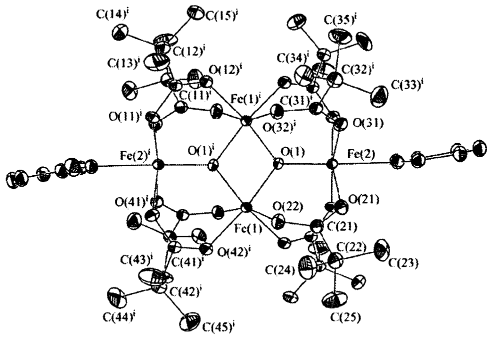

Figure 1. Plot with atomic displacement ellipsoids of **1** showing 90% probability surfaces. Superscript i denotes the atom obtained through the molecular inversion center: $-x + 2$, $-y + 1$, $-z + 1$.

Several other similar complexes have since been investigated in some detail in the literature.[5] The iron-butterfly complexes, which contain a central $[\mathrm{Fe}^{\mathrm{III}}_4(\mu_3\text{-O})_2]^{8+}$ entity, exist in two distinct forms, type I and type II. These are distinguished by the position of the two external- or wing-iron atoms relative to the central planar $\mathrm{Fe}_2(\mu_3\text{-O})_2$ entity. In the situation most often encountered (type II) the two wing-iron atoms are trans relative to the Fe_2O_2 plane, while type I complexes have the two wing Fe on the same side of the Fe_2O_2 plane in a cis configuration. In the iron-butterfly complexes Fe atoms have a bent disposition relative to the central planar Fe_2O_2 entity and thus the μ_3-O atoms must be situated outside of the respective Fe_3 planes. For type-II complexes they sit on opposite sides, and for type-I complexes they sit on the same side of the average plane through all four iron atoms. The complex presented in this paper has a planar disposition of the Fe atoms and thus does not meet the requirements for being labeled a butterfly complex. However, its μ_3-O atoms are situated outside of the respective Fe_3 planes, in this case on either side of the plane through the four iron atoms, and we therefore define the present molecule as being type-II butterfly-like.

The butterfly complexes can be considered to consist of two "fused" μ_3-oxo trinuclear iron carboxylates. We have previously investigated the electron density distributions (EDD) of both mixed-valence and oxidized trinuclear carboxylates.[6] They showed pronounced differences around the μ_3-O atom, and it is therefore interesting to extend the studies of Fe$-$(μ_3-O) bonding to include the butterfly-like variant. This paper contains an analysis and comparison of the experimental and theoretical EDDs in $[\mathrm{Fe}^{\mathrm{III}}_4(\mu_3\text{-O})_2(\mathrm{O_2CCMe_3})_8(\mathrm{NC_5H_4Me})_2]\cdot 2\mathrm{CH_3CN}$, **1**, Figure 1, as well as results of Mössbauer spectroscopic and variable-temperature magnetic susceptibility measurements of **1**.

Table 1. Crystallographic Details of Compound **1**

formula	$Fe_4O_{18}N_4C_{56}H_{92}$
fw	1332.74
cryst system	triclinic
space group	$P\bar{1}$ (No. 2)
Z	1
a, Å	12.693(1)
b, Å	12.913(1)
c, Å	13.473(1)
α, deg	115.372(2)
β, deg	107.702(3)
γ, deg	102.731(2)
V, Å^3	1736.0(3)
T, K	16(5)
ρ, g cm^{-3}	1.196
μ, mm^{-1}	0.89
d_{min}, Å	0.50
N_{meas}, N_{uniq}	55130, 20960
R_{int}	0.025
N_{obs}, N_{var}	14 601, 689
$R(F)$, $R_w(F^2)$, all data	0.022, 0.025
goodness of fit	1.10

Table 2. Selected Bond Distances (Å) and Angles (deg°)[a]

Bond Distances			
Fe(1)$-$O(1)	1.9418(5)	Fe(2)$-$O(1)	1.8532(4)
Fe(1)$-$O(1)^i	1.9404(4)	Fe(2)$-$O(11)	2.0494(5)
Fe(1)$-$O(12)	2.0616(5)	Fe(2)$-$O(21)	2.0561(7)
Fe(1)$-$O(22)	2.0551(7)	Fe(2)$-$O(31)^i	2.0759(5)
Fe(1)$-$O(32)	2.0469(6)	Fe(2)$-$O(41)	2.0391(6)
Fe(1)$-$O(42)^i	2.0691(5)	Fe(2)$-$N(1)	2.2573(5)
C(11)$-$O(11)	1.2825(7)	C(31)$-$O(31)	1.2720(8)
C(11)$-$O(12)	1.2684(9)	C(31)$-$O(32)	1.2745(7)
C(21)$-$O(21)	1.2699(9)	C(41)$-$O(41)	1.2810(7)
C(21)$-$O(22)	1.2747(8)	C(41)$-$O(42)	1.2683(9)
$\langle C-C^{\alpha}\rangle$	1.542(1)	$\langle C^{\alpha}-C^{\beta}\rangle$	1.544(5)

Bond Angles			
O(1)$-$Fe(1)$-$O(1)^i	81.04(2)	Fe(1)$-$O(1)$-$Fe(2)	122.85(3)
Fe(1)$-$O(1)$-$Fe(1)^i	98.96(2)	Fe(1)^i$-$O(1)$-$Fe(2)	123.79(2)

[a] Superscript i refers to the atom obtained from the inversion operation. The Greek superscripting on the C atoms refers to the *tert*-butyl group, $O_2CC^{\alpha}(C^{\beta}H_3)_3$.

Results and Discussion

Structural Analysis of 1. The structure of **1** is displayed in Figure 1, and crystallographic information is given in Table 1. The molecule has a center of symmetry and contains a central $\mathrm{Fe}_4(\mu_3\text{-O})_2$ core, exhibiting two types of Fe with fundamentally different ligand environments; see Table 2.

The Fe atom in the innermost planar (body) Fe_2O_2 region is coordinated to both μ_3-oxygens and furthermore to four pivalate molecules, which bridge the central irons to the wing irons. The wing irons are 0.99 Å above and below the Fe_2O_2 body plane, respectively. A different environment is observed around the wing irons, as they only coordinate to one μ_3-O. These irons also each coordinate to four pivalate ligands, while the sixth ligand, in the trans position to the μ_3-O, is an α-picoline molecule ligated via the nitrogen atom. The bonding geometries around the two different iron sites, which are both nominally iron(III), show pronounced differences, in particular the bond distances to the central O(1). The two Fe(1)$-$O(1) distances are 1.9418(5) and 1.9404(4) Å, which is almost 0.1 Å longer than the Fe(2)$-$O(1) distance of 1.8532(4) Å. The O(1)$-$Fe(1)$-$O(1)^i angle of 81.04(2)° is

---

[5] (a) Armstrong, W. H.; Roth, M. E.; Lippard, S. J. *J. Am. Chem. Soc.* **1987**, *109*, 6318$-$6326. (b) Gorun, S. M.; Lippard, S. J. *Inorg. Chem.* **1988**, *27*, 149$-$156. (c) McCusker, J. K.; Vincent, J. B.; Scmitt, E. A.; Mino, M. L.; Shin, K.; Coggin, D. K.; Hagen, P. M.; Huffman, J. C.; Christou, G.; Hendrickson, D. N. *J. Am. Chem. Soc.* **1991**, *113*, 3012$-$3021. (d) Wemple, M. W.; Coggin, D. K.; Vincent, J. B.; McCusker, J. K.; Streib, W. E.; Huffman, J. C.; Hendrickson, D. N.; Christou, G. *J. Chem. Soc., Dalton Trans.* **1998**, 719$-$725. (e) Çelengil Çetin, R.; Staples, R. J.; Stavropoulos, P. *Inorg. Chem.* **2000**, *39*, 5838$-$5846. (f) Yan, B.; Chen, Z.-D. *Inorg. Chem. Commun.* **2001**, *4*, 138$-$141. (g) Ammala, P.; Cashion, J. D.; Kepert, C. M.; Moubaraki, B.; Murray, K. S.; Spiccia, L.; West, B. O. *Angew. Chem., Int. Ed.* **2000**, *39*, 1688$-$1690.

[6] Overgaard, J. Ph.D. Thesis, Department of Chemistry, University of Aarhus, Aarhus, Denmark, 2001.

far from the ideal octahedral angle of 90°, while the coordination sphere around Fe(2) is less distorted from octahedral symmetry. This may indicate that the two Fe(1) atoms and the two μ_3-O atoms are involved in a four-center interaction which may also account for the unusually short separation of 2.522(1) Å between the μ_3-oxygens. These characteristics suggest that the bonding of two μ_3-O atoms in cis position to Fe(1) decreases the strength of each of the individual Fe(1)−(μ_3-O) interactions compared with the Fe(2)−(μ_3-O) bond, which does not compete with other Fe−(μ_3-O) bonds to the same Fe. Additional support for this point is gained from the presence of a small, but significant, trans effect on Fe(1), which even imparts a conjugation-like distribution of bond lengths in the ligand chains involving the carboxylate groups with C(11) and C(41), namely Fe(1)−O(12)−C(11)−O(11)−Fe(2) and Fe(1)−O(42)−C(41)−O(41)−Fe(2). The other cis-coordinated bridging carboxylate groups involving C(21) and C(31) have identical C−O bonds (see Table 2). The Fe(1)−O(piv) bonds, which are in cis position to both Fe(1)−(μ_3-O) bonds, exhibit bond lengths ($d_{av} = 2.051(6)$ Å) that are slightly shorter than the two trans-coordinated Fe(1)−O(piv) bonds ($d_{av} = 2.065(5)$ Å). The overall average of Fe−O(piv) bond length is 2.057(12) Å. The electronic delocalization in the carboxylate bridges determined through analysis of the C−O bond distances describes two irons in identical oxidation state. Strikingly, the C−O bonds in carboxylate groups C(11) and C(41) as also C(21) and C(31) are pairwise almost exactly similar. A comparison of $C^{\alpha}-C^{\beta}$ bonds of the *tert*-butyl groups shows that they have nearly identical bond distances, as also $C-C^{\alpha}$ have. These observations held together with an impression of the overall shape of the molecule (Figure 1) seem to suggest the presence of a noncrystallographic mirror plane perpendicular to the Fe_2O_2 body plane along the Fe(2)−O(1) bonds. However, a proper crystallographic mirror-plane relationship is contradicted by the orientation of the α-picoline ligand, which is significantly out of this plane. No indications of disorder or increased motion of the outer regions of this ligand is observed, and a search for a space group of higher symmetry was futile. Instead, the extraordinary identity of nonrelated bond distances must be ascribed to the accuracy of the data which can reveal symmetry in bonding in the central part of the molecule.

It is very interesting to note that, in contrast to the case of the basic trinuclear iron carboxylates, the μ_3-oxygens are significantly out of the planes ($d_{\perp} = 0.42$ Å) constituted by the three iron atoms, to which they coordinate.[7] Due to this out-of-plane location, the geometry around O(1) may be described as heavily distorted tetrahedral, although exhibiting Fe−O(1)−Fe angles of 98.96(2) and 123.32(2)°, far from the ideal tetrahedral angle of 109.47°. The sum of the three O(1)−Fe bonds (Σd(Fe−O(1)) = 5.74 Å) is very close to 5.7 Å, a value which has recently been empirically established to apply both to mixed-valence and oxidized trinuclear iron carboxylates.[6] To evaluate more quantitatively the differences in Fe−(μ_3-O) bonding a subsequent section will focus on the electron density distribution.

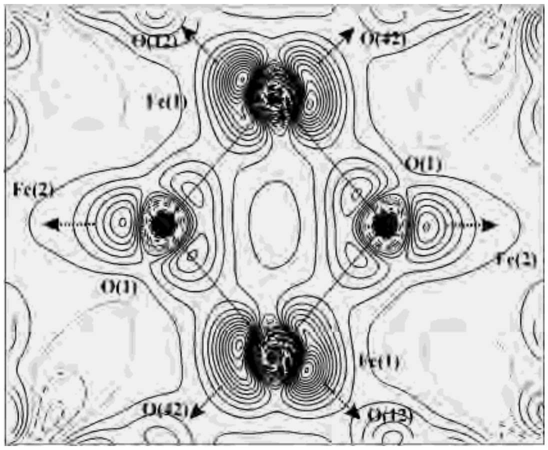

Figure 2. Static model experimental deformation density in central Fe_2O_2 plane. Positive contours are shown with solid lines in intervals of 0.1 e Å^{-3}; negative contours are shown with dashed lines in intervals of 0.5 e Å^{-3}. The zero contour is shown as a dotted line.

Analysis of the Experimental Electron Density Distribution. A multipolar expression was used to describe the electron density distribution.[8] Multipolar, P_v and expansion/contraction parameters κ' of the atoms were least-squares refined against the observed X-ray structure factors. The refined monopoles of the iron atoms substantiate nearly identical oxidation states, as the values are 6.09(2) and 6.14(2) e for Fe(1) and Fe(2), respectively. The monopoles can be used to obtain an estimate of nuclear charge, q, from the relation $q = Z - P_v$, where Z is the number of valence electrons in the unperturbed atomic configuration. This leads to nuclear charges close to +1.9 e for both Fe, significantly less than the nominal value of +3 e. This trend is in accordance with observations in other studies.[9] In agreement with the EDD in trinuclear complexes,[6] the largest oxygen nuclear charge resides on the μ_3-oxygen ($q = -1.08(3)$ e). Charges were also estimated as Bader charges integrated over the volume of the atomic basins.[10] This is the region of space with the property that gradients of the electron distribution terminates at the atomic position and is bounded by a zero-flux surface. This method results in charge values for Fe(1) of +1.76 e, for Fe(2) of +1.67 e, and for the μ_3-oxygen O(1) of −0.91 e. The charge density around O(1) is more expanded than that of the carboxylate oxygens, as evidenced by a κ' value of 0.938(2) for O(1) compared to 0.973(1) for the carboxylate oxygens. The charge clouds around Fe are even more diffuse relative to neutral Fe atoms having κ' and κ'' equal to 0.905(1) and 0.791(8).

A map of the model deformation density, calculated as the static EDD of the model, from which is subtracted the EDD of a superposition of spherical, noninteracting atoms, is shown in Figure 2 for the central Fe_2O_2 region of the molecule. The most conspicuous feature is that the deforma-

---

(7) Blake, A.; Fraser, L. *J. Chem. Soc., Dalton Trans.* **1975**, 193−197. This paper reported a case where the central μ_3-oxygen appears to be significantly out of the Fe_3 plane.

(8) Hansen, N. K.; Coppens, P. *Acta Crystallogr., Sect. A* **1979**, *39*, 909−921.

(9) See for instance: Lee, J.-J.; Lee, G. H.; Wang, Y. *Chem.*−*Eur. J.* **2002**, *8*, 1821−1832.

(10) Volkov, A.; Gatti, C.; Abramov, Yu. A.; Coppens, P. *Acta Crystallogr., Sect. A* **2000**, *56*, 252−258.

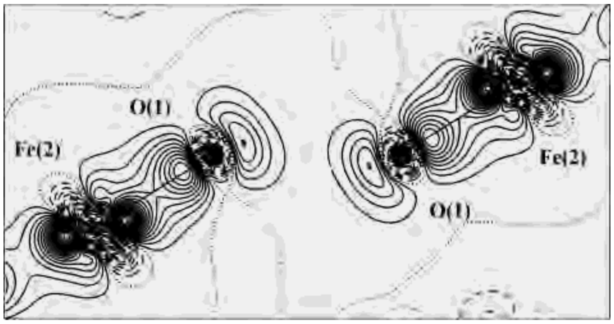

Figure 3. Static model experimental deformation density in Fe(2)−O(1)−O(1)^i plane. Contours are as in Figure 2.

tion density is not only concentrated along Fe−O bonds but forms diffuse areas behind the O(1) atoms extending between Fe(1)−O(1) bonds, thus creating a region of significant electron density in the center of the molecule, a clear manifestation of the proposed four-center interaction involving the two Fe(1) atoms and the two μ_3-oxygens. Furthermore the EDD is markedly less polarized in the O(1)−Fe(1) bonding directions than along O(1)−Fe(2). The latter bond has a peak height of +0.95 e Å^{-3}, while the Fe(1)−O(1) bonds have peaks of close to +0.6 e Å^{-3}. The Fe(2) wing iron atoms lie 0.99 Å above/below the Fe_2O_2 body plane as shown in Figure 3, which depicts the deformation density in the Fe(2)−O(1)−O(1)^i−Fe(2)^i plane perpendicular to the Fe_2O_2 plane of Figure 2. Figure 3 also shows the significant accumulation of electron density on the oxygens in the direction toward the other, symmetry-related O(1). However, this EDD is not exactly on the line between the two oxygens; instead it is slightly above and below. A similar type of deformation density distribution between bridging oxygen atoms was observed in a study of a mixed-valence μ^2-O manganese complex.[11]

Topological Analysis. To further examine the metal−ligand bonding features a topological analysis of the experimental model EDD determined by the multipolar refinement was carried out using the atoms in molecules (AIM) quantum theory.[12] The total electron density topology may be analyzed by a search of characteristic density functions at the critical points where the gradient of the density is zero. Whether such an extremum point is a maximum, a minimum, or a saddle point in the EDD is determined by the sign of the second derivatives of the electron density. In three-dimensional space these derivatives constitute the Hessian matrix, and the trace of this is the Laplacian of the density. Of particular interest are the properties in the bond critical points (bcp) which characterize the bonding interactions in a molecule. Similarly it is of interest to examine the behavior of the negative Laplacian function, $L(r)$. In regions of space where this is positive, electronic charge is accumulated, and where it is negative the charge is depleted. Figures 4 and 5 show the maps of $L(r)$ calculated from the multipolar model on the basis of experimental data in the same planes as selected for Figures 2 and 3.

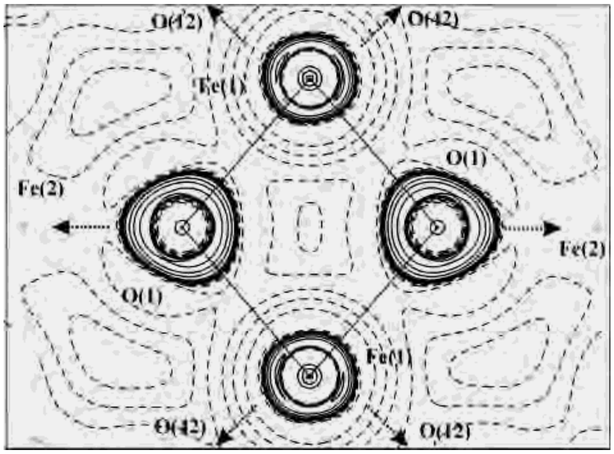

Figure 4. Experimental $L(r)$ distribution in the same section as depicted in Figure 2. Positive contours are shown with solid lines representing the values 2×10^n, 4×10^n, and 8×10^n, where n is in the range −2 to 4. The negative contours are represented by dashed lines showing the values: -2×10^n, -4×10^n, and -8×10^n, with n in the range from −2 to 3. The zero contour is shown with a dotted line.

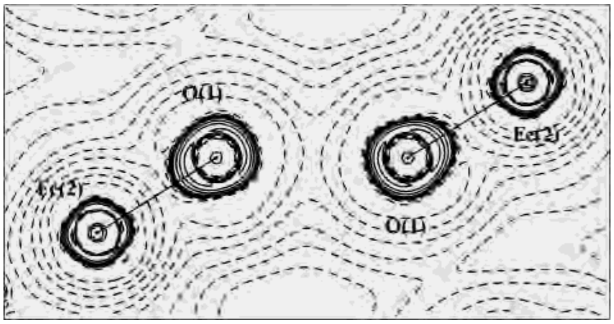

Figure 5. Experimental $L(r)$ distribution in the same section as shown in Figure 3. The contours show the same values as in Figure 4.

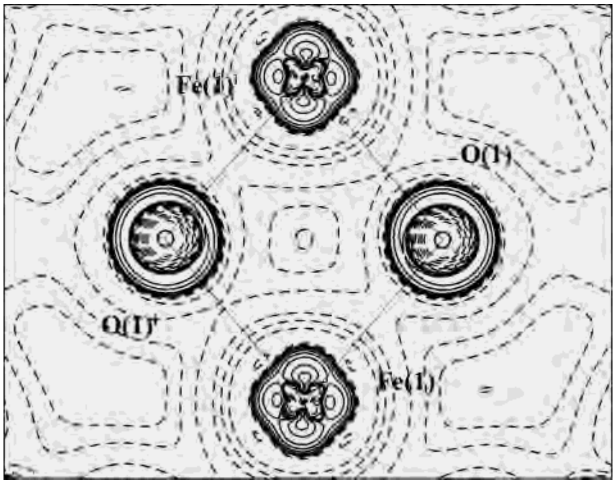

Figure 6. Theoretical $L(r)$ distribution in the same section as depicted in Figure 4. Contours are as in Figure 4.

The theoretical EDD was determined from the result of a DFT single point calculation on the basis of the molecule at the experimental geometry. Figures 6 and 7 show $L(r)$ calculated from the derived theoretical wave function. There is a good agreement between the Laplacian maps from experiment and theory in the vicinity of O(1), which supports the impression of diffuse bonding in the Fe(1)−O(1) direction, in contrast to the stronger, more directional Fe(2)−

---

[11] Jensen, A. F.; Su. Z.; Hansen, N. K.; Larsen, F. K. *Inorg. Chem.* **1995**, *34*, 4244−4252.

[12] Bader, R. F. W. *Atoms in Molecules. A Quantum Theory*; Oxford University Press: New York, 1997.

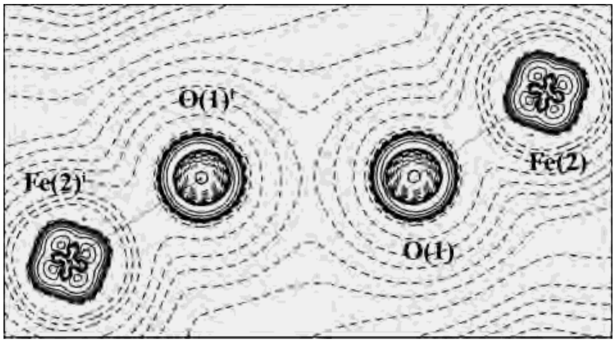

Figure 7. Theoretical $L(r)$ distribution in the same section as depicted in Figure 5. Contours are as in Figure 4.

Table 3. Electron Density Properties at the Lone Pair Maxima (LP) in the Experimental $L(r)$ Distribution around O(1)[a]

atom−LP no.−atom	$\rho(\mathbf{r})$/e Å^{-3}	$\nabla^2\rho(\mathbf{r})$/e Å^{-5}	d(O(1)−LP)/Å	angle/deg
O(1)−1−Fe(2)	6.17	−140.1	0.350	4.2
O(1)−2−Fe(1)^{i}	5.80	−118.1	0.351	17.2
O(1)−3−Fe(1)	5.64	−109.2	0.353	1.3

[a] Inversion i: $-x + 2, -y + 1, -z + 1$.

O(1) bond. Apparently there are only two separate regions exhibiting charge concentrations (so-called valence-shell charge concentrations, or VSCCs) around O(1). One points directly toward Fe(2), see Figure 5, while the other is a very broad distribution (Figure 4), extending toward the two Fe(1) atoms as well as toward the other O(1). However, a more extensive search in the experimental $L(r)$ around O(1) shows that there really are three separable maxima, corresponding to the three Fe−O bonds; see Table 3. The lack of a VSCC above and below the Fe_2O_2 plane on O(1) suggests that O(1) is not involved in any π-interaction with the iron atoms.

Electron counting based on the 18-electron rule concept for transition metals leads to the conclusion that Fe(2) accepts three electrons from O(1) while Fe(1) needs a donation of a total of five electrons from the two O(1). The broad VSCC on O(1) may indicate that this is accomplished not solely by directional bonding but also includes some sort of four-center six-electron interaction. The theoretical calculation, however, does not seem to be able to describe in detail the EDD near the core of the iron atoms, which is evident from a comparison of experimental (Figures 4 and 5) with theoretical (Figures 6 and 7) maps of the Laplacian.

Table 4 lists the topological properties at the bcps in the Fe−ligand bonds calculated from the experimental and theoretical densities. The theoretical values for ρ_{bcp} are all systematically lower than the corresponding experimental values by about 30%, and similarly values of $\nabla^2\rho_{bcp}$ found for the theoretical calculation tend to be lower than experimental values. On the other hand there is generally good correspondence in the position of the bond critical points for theory and experiment. Similar trends are also apparent for the C−O, C−C, and C−N bonds (see Supporting Information). Particularly for the C−O bonds, theory significantly underestimates the value of $\nabla^2\rho_{bcp}$. However, the two sets of values lead to identical conclusions; thus, only the experimental values will be discussed in the remainder of this paper.

Table 4. Topological Properties at Selected Bond Critical Points[a]

bond	ρ_{bcp}	$\nabla^2\rho_{bcp}$	e	r_{1-bcp}	R_{2-bcp}	$G(r_{bcp})$	$V(r_{bcp})$	$H(r_{bcp})$
Fe(1)−O(1)	0.737(4)	11.97(1)	0.05	0.979	0.965	1.04	−1.25	−0.20
	0.48	9.92	0.67	0.984	0.961			
Fe(1)−O(1)^{i}	0.746(5)	12.21(1)	0.04	0.972	0.970	1.06	−1.27	−0.21
	0.46	10.12	0.47	1.007	0.937			
Fe(1)−O(12)	0.528(4)	9.33(1)	0.09	1.041	1.022	0.71	−0.77	−0.06
	0.32	7.79	0.74	1.040	1.032			
Fe(1)−O(22)	0.538(4)	9.14(1)	0.14	1.032	1.027	0.71	−0.79	−0.07
	0.39	8.42	0.04	1.054	1.008			
Fe(1)−O(32)	0.522(4)	9.43(1)	0.07	1.029	1.020	0.71	−0.76	−0.05
	0.40	8.67	0.22	1.051	1.001			
Fe(1)−O(42)^{i}	0.468(5)	8.88(1)	0.10	1.044	1.027	0.64	−0.66	−0.02
	0.29	6.82	0.56	1.054	1.025			
Fe(2)−O(1)	1.111(5)	16.04(1)	0.06	0.935	0.918	1.71	−2.29	−0.58
	0.72	12.43	0.05	1.000	0.857			
Fe(2)−O(11)	0.505(4)	9.47(1)	0.13	1.012	1.038	0.70	−0.74	−0.04
	0.35	8.19	0.50	1.041	1.015			
Fe(2)−O(21)	0.469(4)	8.34(1)	0.11	1.016	1.041	0.62	−0.65	−0.03
	0.33	7.64	0.70	1.053	1.010			
Fe(2)−O(41)	0.461(4)	8.99(1)	0.17	1.028	1.014	0.64	−0.65	−0.01
	0.38	8.54	0.73	1.034	1.010			
Fe(2)−O(31)^{i}	0.470(4)	8.60(1)	0.09	1.037	1.039	0.63	−0.66	−0.03
	0.31	7.01	1.03	1.061	1.010			
Fe(2)−N(1)	0.453(3)	6.05(1)	0.17	1.092	1.166	0.50	−0.57	−0.07
	0.28	4.60	0.03	1.163	1.096			

[a] Units are e Å^{-3} (ρ_{bcp}), e Å^{-5} ($\nabla^2\rho_{bcp}$), Å (r), and hartree Å^{-3} (G, V, H). Second lines show the values from the analysis of the theoretical wave function. Inversion i: $-x + 2, -y + 1, -z + 1$.

The shortest Fe−ligand bond, Fe(2)−O(1), has the largest density in the bcp, $\rho_{bcp} = 1.111(5)$ e Å^{-3}, implying that this bond is of considerable strength. The value is significantly higher than the corresponding values in the Fe−(μ_3-O) bonds in related basic trinuclear iron carboxylates,[6] which exhibit values of ρ_{bcp} in the range from 0.77 to 0.92 e Å^{-3}. The Fe(2)−O(1) bond also has the most positive Laplacian of all Fe−ligand bonds, suggesting that it has the most electrostatic character and thus relatively the least significant covalent contribution of the 12 Fe−ligand bonds. A closer inspection of the values of $\nabla^2\rho_{bcp}$ in Table 4 reveals an exponential increase with diminishing value of the corresponding bond lengths, R_{ij}, a tendency also observed in the topological analysis of the EDD in hydrogen bonds.[13] To examine this relationship in more detail, we have pooled the experimental results of topological analysis of three other iron−carboxylate complexes[6] with the results from this study. The striking correlation is shown in Figure 8. Thus, a shorter bond corresponds to a more positive value for $\nabla^2\rho_{bcp}$. This differentiates the metal−ligand bonds of electrostatic nature from covalent bonds, which get a more negative value of $\nabla^2\rho_{bcp}$ the shorter they become. In the extreme case for very short Fe−ligand bonds, conceivably, the character of the bond would become predominantly covalent as the electron density enters the region between the atoms and one would then expect the $\nabla^2\rho_{bcp}$ to change from positive to negative value.

Another measure for the bond strength can be obtained from the energy densities, which for closed-shell interactions can be estimated by the semiempirical relation proposed by Abramov.[14] The local kinetic energy density distribution, G,

---

(13) Espinosa, E.; Souhassou, M.; Lachekar, H.; Lecomte, C. *Acta Crystallogr., Sect. B* **1999**, *55*, 563−572. Espinosa, E.; Alkorta, I.; Elguero, J.; Molins, E. *J. Chem. Phys.* **2002**, *117*, 5529−5542.

(14) Abramov, Yu. A. *Acta Crystallogr., Sect. A* **1997**, *53*, 264−272.

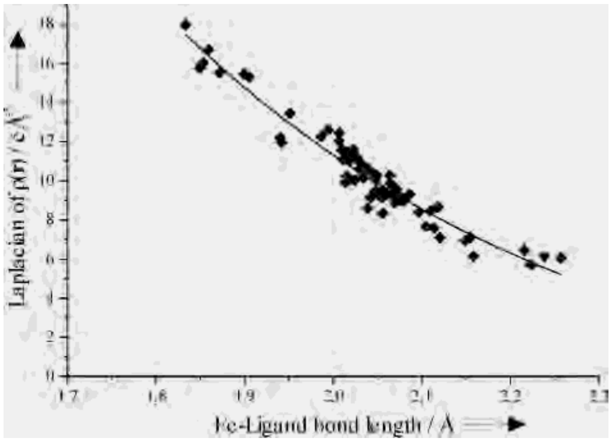

Figure 8. Experimental values of $\nabla^2\rho_{bcp}$ as function of bond length for Fe−ligand bonds in four different complexes.[6] The first-order exponential decay fit is shown with a solid line ($L(r) = -3.4 + 20.8 \exp\{-(d(\mathrm{Fe-L}) - 1.833)/0.48\}$).

Table 5. d-Orbital Populations

	$d(z^2)$	$d(xy)$	sum	$d(xz)$	$d(yz)$	$d(x^2 - y^2)$	sum
Fe(1)	1.37	1.32	2.69	1.18	1.00	1.22	3.40
Fe(2)	1.50	1.03	2.53	1.49	1.28	0.85	3.62

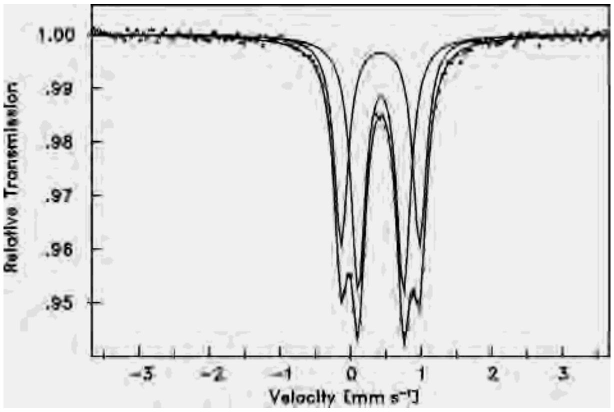

Figure 9. Mössbauer spectrum measured at 293 K of **1**.

evaluated at the bcp, reflects the tendency to move electrons away from the interatomic regions and gives a measure for the electrostatic contribution to the bond energy. The potential energy density, V, quantifies the inclination for electrons to accumulate in the bonding regions; i.e., it is a measure for the covalency of the bond. The Fe(2)−O(1) exhibits the largest value of G of all Fe−ligand bonds (Table 4). At the same time there is a large negative value of the potential energy density, V, at this bond critical point, such that the total energy density, H, is the most negative for the Fe(2)−O(1) bond. This leads to the conclusion that the Fe(2)−O(1) bond possesses the largest electrostatic as well as considerable covalent contributions to the total energy.

Orbital Populations on Fe. The d-orbital populations on each metal atom site can be extracted from the refined multipolar population parameters.[15] Table 5 lists the results according to a choice of axes directions defined so that on Fe(1) the unique axis is nearly perpendicular to the Fe_2O_2 plane (z points toward O(22)). The x axis points toward the symmetry-related Fe(1) and thus the x and y axes point approximately between the Fe−ligand directions. The distorted octahedral geometry around Fe(1) (Table 2) lowers the correspondence between the Fe−ligand bonds and the local orthogonal coordinate system of Fe(1). For Fe(2), the z axis is chosen to point toward O(1), and the x and y axes are directed approximately between the pivalate oxygen ligands. Using this choice of axes makes the $d(z^2)$ and $d(xy)$ the energetically destabilized orbitals. First of all, Table 5 shows the existence of a high-spin configuration indicated by the presence of electrons in all five d orbitals on both irons. This finding was confirmed by Mössbauer measurements. The $d(z^2)$ orbital is significantly overpopulated on both Fe(1) and Fe(2), suggesting an appreciable σ-donation from pivalate ligands and O(1), respectively. On the other hand, marked differences stand out in the $d(xy)$ orbital, indicating that the σ-donation from O(1) to Fe(1) is significantly larger than the corresponding donation from the pivalate oxygens to Fe(2). It seems that no π-interaction between O(1) and Fe(1) is present, as such phenomenon would increase the population in the $d(xz)$ and $d(yz)$ orbitals to contain more than one electron each. On the other hand, some sort of π-interaction seems to occur between Fe(2) and O(1), illustrated by the significant occupation of the involved $d(xz)$ and $d(yz)$ orbitals on Fe(2). Finally, there is a clear difference between the occupation of the $d(x^2 - y^2)$ orbitals on the two irons. If a more diffuse bonding exists in the body-Fe_2O_2 region, then that would involve the $d(x^2 - y^2)$ orbital on Fe(1), which indeed seems well-populated. Thus, although the two irons have the same amount of valence electrons, their distributions appear clearly different, corroborating the observations from the structural and topological analysis.

Mössbauer Spectroscopy. Mössbauer spectroscopy is a particularly suitable method to study chemical bonding interactions in iron complexes, since two parameters of a spectrum can be related directly to populations of valence shell orbitals. The isomer shift relates the total electron density on the iron atom and the quadrupole splitting reflects any asymmetry in the distribution of the electron density. The Mössbauer spectrum of **1,** collected at 293 K, is shown in Figure 9. The spectrum clearly shows two well-resolved doublets, originating respectively from the wing- and body-iron atoms of the $Fe_4(\mu_3\text{-}O)_2$ core, which, in accordance with the symmetry of the molecule, were fitted to two equal-area doublets. While the isomer shifts (δ) for both doublets are similar with 0.428 and 0.421 mm/s, the quadrupole splittings (ΔE_Q) are quite different with 0.637 and 1.102 mm/s, respectively. The values for δ are within the range expected for iron(III) high spin and comparable to those of other complexes with Fe_4O_2 butterfly cores.[5a−c] The difference between the ΔE_Q values is smaller than for a similar type II butterfly complex ($[Fe_4O_2(piv)_8(DMSO)_2]$:[16] IS (δ) = 0.55 mm/s; QS (ΔE_Q) = 0.62 and 1.45 mm/s) but clearly larger than reported for other iron(III) compounds with Fe_2O_4 cores.[5a−c]

---

(15) Holladay, A.; Leung, P.; Coppens, P. *Acta Crystallogr., Sect. A* **1983**, *39*, 377−387.

(16) Rentschler, E.; Weyhermüller, T.; Timco, G. A. *ESF Conference 2001, Davos: Molecular Magnets*; 2001.

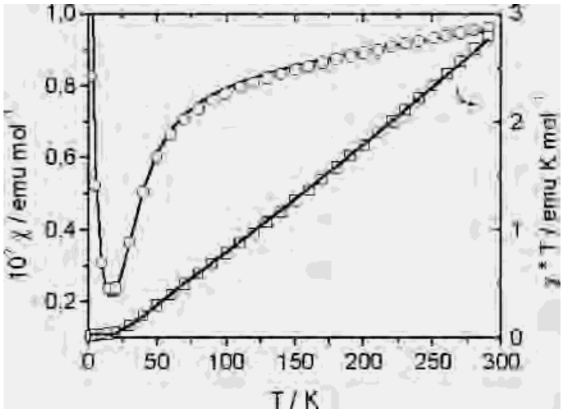

Figure 10. Variable-temperature magnetic susceptibility measurement of **1**.

The contribution of the nonbonding part $(V_{zz})_{nb}$ to the electric field gradient (EFG) is negligible for a high-spin iron(III); the ΔE_Q values therefore reflect directly differences in the bonding characteristics of the ligands, the number of each type of ligand, and their relative disposition. The overall electronic density is comparable for both sites in **1**, as shown by comparable isomer shifts; thus, different σ-basicities of the ligands are reflected by the quadrupole splitting parameters. In particular, Fe(1) exhibits an O_6 coordination sphere with distances of ⟨Fe(1)−O(piv)⟩ 2.058(9) Å and Fe(1)−O(1) 1.9418(5) Å a much more symmetric coordination environment than Fe(2) has. The wing-iron atom, Fe(2), shows a NO_5 coordination with O(1) and N lying on a unique axis with distances Fe(2)−O(1) = 1.8532(4) Å and Fe(2)−N = 2.2573(5) Å, while the average distance ⟨Fe(2)−O(piv)⟩ of 2.055(16) Å is the same as for Fe(1). The Mössbauer signal for Fe(1) is therefore assigned to the smaller ΔE_Q value of 0.637 mm/s, whereas the doublet showing a ΔE_Q value of 1.102 mm/s is assigned to the Fe(2) ion.

Magnetic Susceptibility Measurements. The result of the temperature-dependent magnetic susceptibility measurement is shown in Figure 10. At room temperature the value of the χT product is 3.0 emu K mol^{-1}, a value far below the theoretical value for four uncoupled iron (III) ions (4 × 4.375 emu K mol^{-1}), indicating fairly strong antiferromagnetic interaction between the spin centers. With lowering temperature χT decreases further, reaching a value close to zero at 20 K. The overall temperature dependence can be described by the use of the Heisenberg−Dirac−van Vleck Hamiltonian:

$$H = -2J_{wb}(S_1\cdot S_2 + S_2\cdot S_1^{i} + S_1\cdot S_2^{i} + S_1^{i}\cdot S_2^{i}) - 2J_{bb}(S_1\cdot S_1^{i})$$

Here J_{wb} describes the "wing−body" exchange interaction and J_{bb} describes the "body−body" interaction and the numbering scheme for $(S_i\cdot S_j)$ follows the labels used in Figure 1.

A best fit to the experimental curve gave $J_{wb} = -37.2$ cm^{-1}; a paramagnetic impurity of 0.017% was taken into account. For J_{bb} values between 3 and −7 cm^{-1} do not change apparently the goodness of fit; therefore, J_{bb} was assumed to be zero. In Figure 11 is shown the error surface for the J_{wb}−J_{bb} coupling constants, confirming the wide range of possible values for J_{bb}. This uncertainty of the coupling between the core iron atoms is well-known from butterfly structures and results from spin frustration of the centered spins.[5] The interaction J_{wb} dominates the magnetic structure thus the intrinsic character of the J_{bb} interaction is negated.

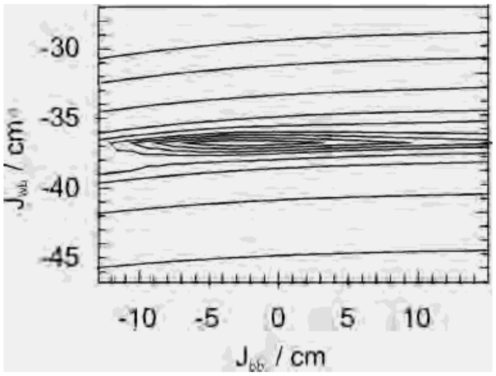

Figure 11. Error surface for the two coupling constants J_{bb} vs J_{wb} for the simulation of the magnetic susceptibility measurement of **1**.

Conclusion

The analysis of both theoretical and experimental electron density distributions of the iron complex **1** has revealed significantly different bonding interactions in the iron−ligand bonds for the two iron atoms. A very directional bonding from the μ_3-bridging oxygen to one iron is contrasted by a weaker, more diffuse interaction to the other iron. The experimentally derived iron d-orbital populations and local energy density distributions support the differences observed in the topological analysis of the Fe−(μ_3-O) bonds. Additional support is gained from the results of Mössbauer spectroscopy. Since the high-spin Fe^{3+} ion has an ^6S electronic ground state and is spherically symmetric, any electric field gradient arises solely from changes in the surrounding of the nucleus. The differences in the quadrupolar splittings of the two iron sites results from the anisotropy of covalency as confirmed by the analysis of the electron density distributions. Thus, the Mössbauer spectrum nicely reflects the less polarized bonding density in the Fe(1)−O(1) direction and the fact that Fe(2)−O(1) bond possesses the largest electrostatic and covalent contributions.

The topological analysis of the experimental electron density distribution revealed a clear relationship between the bond length of an iron−ligand bond and the value of the Laplacian at the bond critical point. This relationship will be the subject of further studies in our laboratories.

Experimental Section

Synthesis. The cluster compound $[Fe_4(\mu_3\text{-}O)_2(O_2CCMe_3)_8(NC_5H_4\text{-}Me)_2]\cdot 2CH_3CN$ was obtained from $[Fe_3(\mu_3\text{-}O)(O_2CCMe_3)_6(HO_2\text{-}CCMe_3)_3]$ (**A**). The synthesis and structure of compound **A** has been reported elsewhere.[17]

Compound 1: $[Fe_4(\mu_3\text{-}O)_2(O_2CCMe_3)_8(NC_5H_4Me)_2]\cdot 2CH_3CN$. Compound **A** (3.0 g) was dissolved in α-picoline (C_6H_7N, 6.0 mL)

---

(17) (a) Gerbeleu, N. V.; Timco, G. A.; Turta, K. I.; Popovich, G. A.; Bobkova, S. A.; Indrichan, K. M. *Zh. Neorg. Khim.* **1986**, *31*, 684−690. (b) Wilson, C.; Iversen, B. B.; Overgaard, J.; Larsen, F. K.; Wu, G.; Palii, S. P.; Timco, G. A.; Gerbeleu, N. V. *J. Am. Chem. Soc.* **2000**, *122*, 11370−11379.

by heating at 80 °C. The hot solution was diluted with CH_3CN (30 mL) and stirred for 0.5 h exposed to air.[18] The solution was then cooled to room temperature. Diethyl ether (20 mL) was added and the solution filtered. The red-brown solution was allowed to slowly evaporate in a flask that was partially open to air. After approximately 2 days red-black crystals in a yield of 1.9 g were obtained. Compound **1** can also be obtained from $[Fe_3O(O_2CCMe_3)_6(H_2O)_3]{\cdot}O_2CCMe_3$ using the same synthesis procedure described above. The synthesis of $[Fe_3O(O_2CCMe_3)_6(H_2O)_3]{\cdot}O_2CCMe_3$ has been reported previously.[19] Anal. Calcd for **1** ($C_{56}H_{92}O_{18}N_4Fe_4$): C, 50.47; H, 6.96; N, 4.20. Found: C, 49.81; H, 6.95; N, 3.75.

Single-Crystal X-ray Diffraction. A red-black single crystal ($0.15 \times 0.12 \times 0.08$ mm^3) was mounted on a thin glass fiber using epoxy glue. The glass fiber was glued to a copper wire that was soldered to a brass pin. The whole assembly was mounted on a 4-circle diffractometer, and the crystal was centered in an X-ray beam with a wavelength, λ, of 0.643 Å at the synchrotron beamline X3A1 at NSLS, The National Synchrotron Light Source at Brookhaven National Laboratory, Upton, NY. The beamline is equipped with a Bruker SMART6000 CCD detector, the surface of which was positioned at a distance of 3.24 cm from the crystal and at a 2θ angle of $-30°$. Approximately 2000 frames were collected using the φ-axis of the diffractometer ($\Delta\varphi = 0.3°$) as rotation axis. A total of 55 130 integrated intensities were obtained using the program SAINT+.[20] Systematic intensity variations between symmetry related reflections were analyzed with program SADABS[20] and used for a correction. Significant outliers were identified and rejected, and the remaining reflections were averaged to 20 960 unique reflections with SORTAV.[21] The internal agreement factor was 0.025. Further details are available in Table 1.

X-ray Data Modeling. It has previously been identified that data collected by area detector may contain outliers.[22] We therefore decided to discard singly measured reflections which reduced the number of unique reflections to 17 886. The structure was solved from direct methods as implemented in SHELXS,[23] and an initial high order (HO) refinement using 7786 reflections with $(\sin\theta)/\lambda$ values above 0.7 Å^{-1} established the structural model shown in Figure 1. On the basis of this model, 879 reflections were discarded as significant outliers. Of these, only 58 reflections were observed at a 2σ level. It is worth mentioning that all hydrogen atoms even of the *tert*-butyl groups could be located from a difference Fourier synthesis following the initial structural refinement, emphasizing the high quality of the data. To test the validity of this structural model, Hirshfelds rigid bond test was employed.[24] A mean value of $\Delta_{A-B} = 5.7$ pm^2 for all bonds, including the Fe−ligand bonds, is significantly below the threshold of 10 pm^2, which is taken to indicate a rigid bond. This structural description was therefore maintained in the following multipolar refinements using all reflections ($I > 2\sigma(I)$) with the program XD.[25] Ionic scattering factors were chosen for the iron atoms (Fe^{3+}). In the refinement procedure, the level of multipolar functions was incremented step by step. The final model included hexadecapoles ($l = 4$) on Fe and octopoles ($l = 3$) on all O, N, and C atoms, while all the hydrogens were assigned a common monopole and a dipole directed toward its nearest neighbor. After the final level of multipoles was reached, a refinement of only the κ'' parameters was performed, and these parameters were then fixed in a final refinement. All the H atoms in **1** were moved to a distance of 1.06 Å (1.08 Å) from the methyl carbon (aromatic carbon) atom to which they bond, and the SDS scattering factor for hydrogen was used.[26] Each atom type was assigned separate radially modifying κ' parameters, with the exception that O(1) was treated independently of the other oxygens. A description with individual radial dependency for the two Fe gave unrealistic results. Similarly, the effect of separating the κ' parameters for the methyl carbons from the other carbons was examined. This was found to result in a significant charge transfer from the hydrogens to the methyl carbons, however maintaining the overall charge on the CH_3 entities. This model was not used. A constraint on the monopoles ensured that the solvent acetonitrile molecule and the iron complex remain neutral throughout the refinement procedure. The final model fitted the data well, as shown by the residual density maps in the Fe-containing planes (Figure 12a,b) and the agreement indices ($R_w(F^2) = 0.024$ and the goodness of fit = 1.10 for 14 601 observed reflections and 689 parameters).

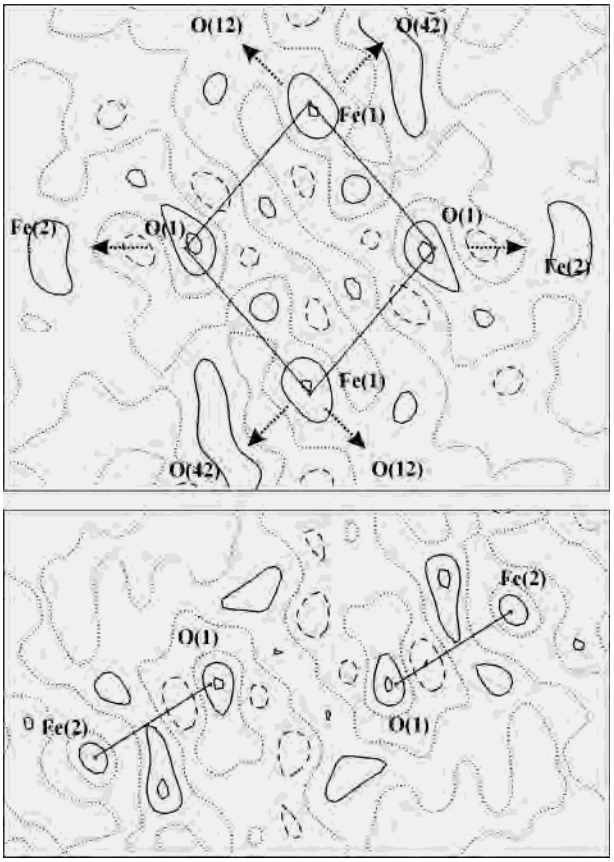

Figure 12. Residual density in the same sections as shown in (top) Figure 2 and (bottom) Figure 3. Positive contours are shown with solid lines in intervals of 0.1 e Å^{-3}; negative contours are shown with dashed lines in intervals of 0.1 e Å^{-3}. The zero contour is shown as a dotted line.

DFT Single Point Calculation. A single point calculation in the experimental geometry was performed using density functional

---

[18] When synthesis was carried out in an inert atmosphere, the mixed-valence asymmetric compound $[Fe_3(\mu_3\text{-}O)(O_2CCMe_3)_6(NC_5H_4Me)_2(HO_2CCMe_3)](CH_3CN)$ was isolated; see ref 6.

[19] Batsanov, A. S.; Struchkov, Yu. T.; Timco, G. A. *Russ. J. Coord. Chem.* **1988**, *14*, 266−270.

[20] Sheldrick, G. S. *SAINT+*; University of Göttingen: Göttingen, Germany, 1997.

[21] Blessing, R. H. *J. Appl. Crystallogr.* **1997**, *30*, 421−426.

[22] Iversen, B. B.; Larsen, F. K.; Pinkerton, A. A.; Martin, A.; Darovsky, A.; Reynolds, P. A. *Acta Crystallogr., Sect. B* **1999**, *55*, 363−374.

[23] Sheldrick, G. M. *SHELX-86. Program for crystal structure solution*; University of Göttingen: Göttingen, Germany, 1986.

[24] Hirshfeld, F. L. *Acta Crystallogr.* **1976**, *A32*, 239−244.

[25] Koritsanszky, T.; Howard, S. T.; Richter, T.; Mallinson, P. R.; Su, Z.; Hansen, N. K. *XD. A Computer Program Package for Multipole Refinement and Analysis of Charge Densities from X-ray Diffraction Data*; Free University of Berlin: Berlin, 1995.

[26] Stewart, R. F.; Davidson, E. R.; Simpson, W. T. *J. Chem. Phys.* **1965**, *42*, 3175.

theory as implemented in Jaguar 4.0 (release 23).[27] The AIMPAC suite of programs was used for the topological analysis of the theoretical wave function.[28] The calculation was done using the B3LYP hybrid method[29] and the Los Alamos[30] LACV3P basis set, which is a triple-ζ basis set that places effective core potentials on the iron centers and uses Pople type 6-311g on all other atoms.[31]

Mössbauer Spectroscopy Measurements. The Mössbauer spectrum was recorded on a constant-acceleration conventional spectrometer with a ^{57}Co/Rh source. Isomer shifts are given relative to α-iron at room temperature. The absorber was a sample (100−130 mg) of a microcrystalline powder at room temperature enclosed in an 18 mm diameter plastic sample holder.

Magnetic Susceptibility Measurements. Temperature-dependent magnetic susceptibility measurements were performed with a Quantum Design SQUID magnetometer MPMS in the temperature range 2−298 K in an applied magnetic field of 1 T. The experimental data were corrected for the diamagnetic contribution using Pascal's constants.

Acknowledgment. The SUNY X3 beam line at National Synchrotron Light Source (Brookhaven National Laboratory, Upton, NY) is supported by the Division of Basic Energy Sciences of the U.S. Department of Energy (Grant DE-FG02-86ER45231). The synchrotron work is supported by a DANSYNC grant from the Danish Research Council. Research scientist Dr. Guang Wu at SUNY X3, NSLS, is thanked for helpful assistance during data collection and for providing additional software for the data reduction. G.A.T. thanks the Danish Natural Science Research Council for a postdoctoral employment paid by the DANSYNC grant. The authors thank the Australian Centre for Advanced Computing and Communications (ac3) [http://www.ac3.com.au] for a generous allocation of computer resources. D.E.H. also thanks the Australian Research Council.

Supporting Information Available: A crystallographic CIF file, a table of topological properties in all bonds in **1**, and lists of refined multipolar parameters. This material is available free of charge via the Internet at http://pubs.acs.org.

IC034062C

---

(27) *Jaguar 4.0*; Schrodinger Inc.: Portland, OR, 2000.

(28) Biegler-König, F. W.; Bader, R. F. W.; Tang, T.-H. *J. Comput. Chem*. **1982**, *3*, 317−328.

(29) (a) Becke,. A. D. *J. Chem. Phys.* **1993**, *98*, 5648. (b) Lee, C.; Yang, W.; Parr, R. G. *Phys. Rev. B* **1988**, *38*, 3098. (c) Stevens, P. J.; Devlin, F. J.; Chabalowski, C. F.; Frisch, M. J. *J. Phys. Chem.* **1994**, *98*, 11623. (d) Adamo, C.; Barone, V. *Chem. Phys. Lett*. **1997**, *274*, 242.

(30) (a) Hay, P., J.; Wadt, W. R. *J. Chem. Phys*. **1985**, *82*, 270. (b) Wadt, W. R.; Hay, P. J. *J. Chem. Phys.* **1985**, *82*, 284. (c) Hay, P. J.; Wadt, W. R. *J. Chem. Phys*. **1985**, *82*, 299.

(31) (a) Krishnan, R.; Binkley, J. S.; Seeger, R.; Pople, J. A. *J. Chem. Phys*. **1980**, *72*, 5639. (b) Mclean, A. D.; Chandler, G. S. *J. Chem. Phys*. **1980**, *72*, 650.